Aerospace Science and Technology 46 (2015) 273–281

Contents lists available at ScienceDirect

Aerospace Science and Technology

www.elsevier.com/locate/aescte

Active cancellation analysis based on the radar detection probability

Mingxu Yi, Lifeng Wang *, Jun Huang

School of Aeronautic Science and Technology, Beihang University, Beijing 100191, China

ARTICLE INFO

Article history:
Received 30 May 2014
Received in revised form 14 December 2014
Accepted 22 July 2015
Available online 30 July 2015

Keywords:
Active stealth
Active cancellation
Linear frequency modulation (LFM)
Nonlinear frequency modulation (NLFM)
Detection probability
Signal-to-noise ratio (SNR)

ABSTRACT

In this paper, a cancelling system for linear and three nonlinear frequency modulated signals is proposed. According to the RCS (Radar Cross Section) characteristic of target, amplitude and phase modulation are made to acquire the signal having the same frequency as the echo pulse but with the opposite phase. This signal cancels the radar echo signal. The basic theory of active cancellation stealth is introduced. Based on two kinds of radar target fluctuation models (Swerling I and Swerling III), the formulas of radar detection probability are given. The influence of amplitude, phase and frequency error on the radar detection probability have been discussed. Simulation results show that the technology of active cancellation stealth is feasible in theory, it could reduce the radar detection probability.

1. Introduction

Radar cross section reduction techniques of aircraft generally fall into one of four categories [1,2]: materials selection and coating, target shaping, passive cancellation and active cancellation. Active cancellation stealth is a significant research direction in the field of stealth. In contrast with traditional stealth, the radar detection probability of the target to be protected could be reduced further by active cancellation stealth [3–6]. The high speed microelectronic devices, phased-array antenna techniques, and computer processing have made active cancellation stealth techniques more feasible and practical.

Two signals in free space may generate coherent interference which makes the synthesized signal weaker or stronger. During the research of signal cancellation, more attention has been paid to radar interference signal or clutter [7–9], acoustic signal [10–12], linear frequency modulation pulse compression signal [13,14]. LFM pulse compression signal is utilized worldwide in modern radar systems. NLFM signal is a general class of continuous phase coding in which the sweep rate is not restricted to a constant. NLFM signals are also applied to many kinds of radar systems [15]. Consequently, the interference on LFM and NFLM radar has become an important content of modern electronic techniques.

The earliest expressions for the probability of detection for constant target reflections were provided by Marcum [16]. Swerling [17] introduced techniques for modelling target fluctuation to account for the usual variation in the target radar cross section. He proposed four different models that have been combined and generalized by using a parameterized gamma distribution. In this work, we present a cancelling system for the LFM and three NLFM signals (Taylor window [18], Combination LFM and Tangent-FM [19], Stepped NLFM [20]). We also discuss the effect of amplitude, phased and frequency error on the radar detection probability under the models Swerling I and Swerling III.

2. LFM signal and NLFM signal

An arbitrary FM chirp signal can be given as

$$S(t) = a(t)\exp\left[j\varphi(t)\right] \tag{1}$$

where $a(t)$ denotes the amplitude modulation function, $\varphi(t)$ denotes the phase modulation function, and the corresponding instantaneous frequency function is

$$f(t) = \frac{1}{2\pi}\frac{d\varphi}{dt} \tag{2}$$

Suppose the envelope is rectangular, then we have $a(t) = 1$.

The expression of complex baseband signal of LFM is [13]

$$S(t) = \exp\left(j\pi\mu t^2\right) \tag{3}$$

where $\mu = B/T$ is called as slope of frequency modulation, B is the bandwidth, T is the pulse duration.

To generate the NLFM signal, it is necessary to obtain the frequency function $f(t)$ which determines the spectrum shape. In this paper, we consider three different NLFM waveforms as follows:

* Corresponding author. Tel.: +86 18201311103.
E-mail address: wanglf1972@163.com (L. Wang).

http://dx.doi.org/10.1016/j.ast.2015.07.018

Table 1
Optimal setting of α and γ.

Name	α	γ
$B \geq \frac{35}{T}$	$0.88 \leq \alpha \leq 0.94$	$1.42 \leq \gamma \leq 1.52$
For small bandwidth chirps	$0.88 \leq \alpha \leq 1$ or $0.66 \leq \alpha \leq 0.84$	$0.6 \leq \gamma \leq 1.08$ or $1.12 \leq \gamma \leq 1.44$

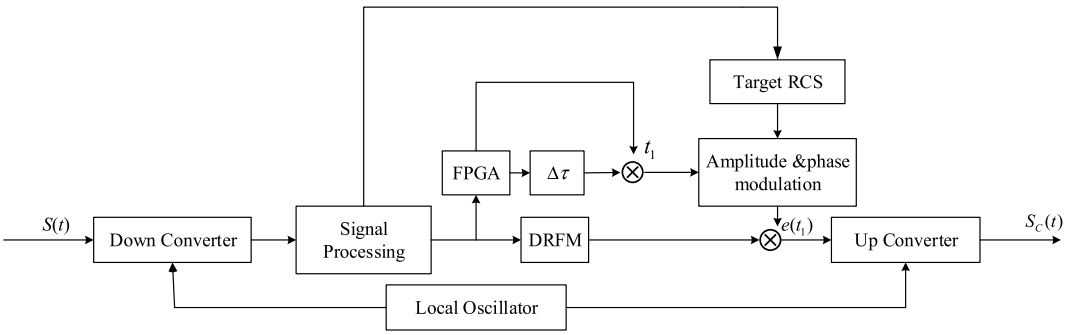

Fig. 1. Block diagram of cancellation signal.

(1) Taylor window shape

The Taylor weighting function $f(t)$ can be expressed in Fourier series as follows

$$f(t) = \frac{Bt}{T} - \frac{B}{2} + \sum_{n=1}^{\infty} A(n) B \sin\left(\frac{2\pi nt}{T}\right) \tag{4}$$

where $A(n)$ is the coefficient of the infinite series. In practice, Eq. (4) can be terminated at finite terms. Therefore, the phase function is given by

$$\varphi(t) = \frac{\pi Bt^2}{T} + 2BT \sum_{n=1}^{N} \frac{A(n)}{n} \sin^2\left(\frac{\pi nt}{T}\right) \tag{5}$$

where $N = 10$.

(2) Combination of LFM and Tangent-FM

The frequency modulation function in radians of the combination of LFM and Tangent-FM function can be written as

$$\frac{d\varphi}{dt} = \pi B\left[\frac{\alpha}{\tan\gamma} \tan\left(\frac{2\gamma t}{T}\right) + \frac{2(1-\alpha)t}{T}\right] \tag{6}$$

where the constant γ controls the proportion of the tangent curve which is used and α controls the balance between LFM and Tangent-FM. The optimal setting of α and γ for various range bandwidth chirps are shown in Table 1 [21].

Integrating Eq. (6), we get

$$\varphi(t) = \frac{\pi B}{T}(1-\alpha)t^2 - \frac{\pi B\alpha T}{2\gamma \tan\gamma} \ln\left|\cos\frac{2\gamma}{T}t\right| \tag{7}$$

(3) Stepped NLFM waveform

Let the nonlinear frequency characteristic of the evaluated signal be expressed as

$$f(t) = \frac{t}{T}\left[B_L + \frac{B_C}{\sqrt{1 - 4t^2/T^2}}\right] \tag{8}$$

where B_L is the total frequency sweep of the LFM part and B_C is the total frequency sweep of the NLFM part. The phase modulation function is given by

$$\varphi(t) = \frac{\pi B_L t^2}{T} - \pi B_C \sqrt{\left(\frac{T}{2}\right)^2 - t^2} \tag{9}$$

3. LFM and NLFM signal cancelling system

The block diagram of the LFM and NLFM signal cancelling system is shown in Fig. 1. Since the variations of radar signal frequency and target's attitude, the echo phase modulation changes as time varies. The variation of signal frequency of radar can be detected by radar detector system, and the variation of target's attitude can be got from its complex RCS.

In Fig. 1, $S(t)$ represents the transmitted radar signal, $S_C(t)$ is the cancellation signal, $e(t_1)$ is the jamming signal. τ_1 is the time delay between the time when the radar signal is received and the time when the cancellation signal is transmitted. $\Delta\tau$ is the jammer processing delay time. The functions of this system mainly include two parts: on one hand, after down conversation, the radar signal is sent to a digital radio frequency memory (DRFM) storage [14]. On the other hand, the delay time τ_1 at a particular instant of time t_1 is controlled by the field programmable gate array (FPGA) chip, and the received signal is multiplied by the conjugation of its delayed version ($\Delta\tau$ is also controlled by FPGA). Then, multiplying the results to obtain the jamming signal. Based on the target's RCS, amplitude and phase modulation are made in order to obtain the signal having the same amplitude and frequency as the echo pulse but with the opposite phase [4,13]. This signal cancels the radar echo signals.

The position of targets includes range, angle are obtained by using the block diagram of signal processing which is given by Fig. 2 in details. The target's range, R, is calculated by measuring the time delay Δt, it takes a pulse to travel the two-way path between radar and target. The system uses Doppler frequency to obtain the target radial velocity, as well as to distinguish between moving and stationary objects such as clutter. The amplitude and phase information of the radar signal can be got by using the orthogonal detector which is shown in Fig. 3.

The jamming signal $e(t_1)$ is given by

$$e(t_1) = S(t_1) \times S^*(t_1 - \Delta\tau) \cdot a_{RCS} \cdot \exp\left[j(\varphi_{RCS} + \pi)\right]$$

where φ_{RCS} and a_{RCS} denote the target's RCS phase and amplitude characteristic, respectively. "*" denotes the complex conjugate of the function. Let $S(t_1) = S(t - \tau_1)$, so the cancellation signal $S_C(t)$ can be expressed as follows

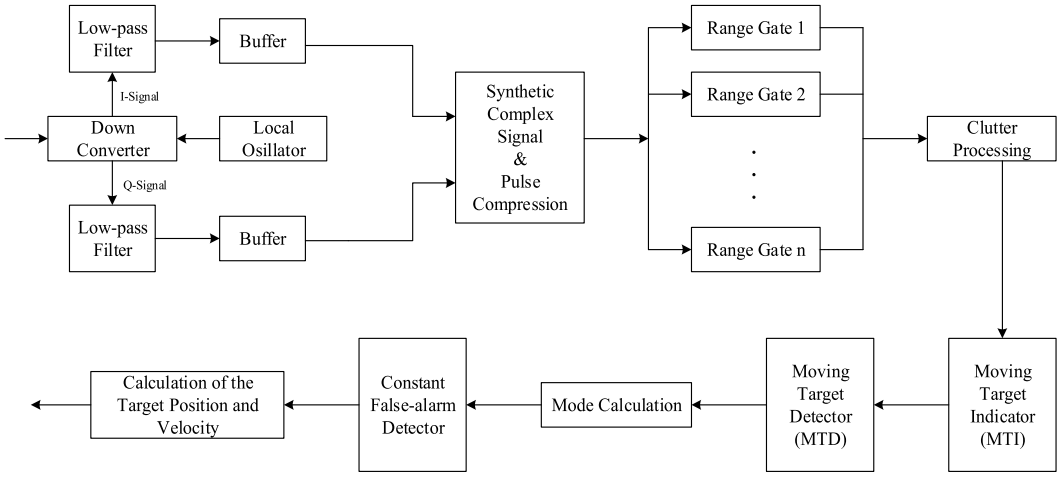

Fig. 2. Block diagram of radar signal processing.

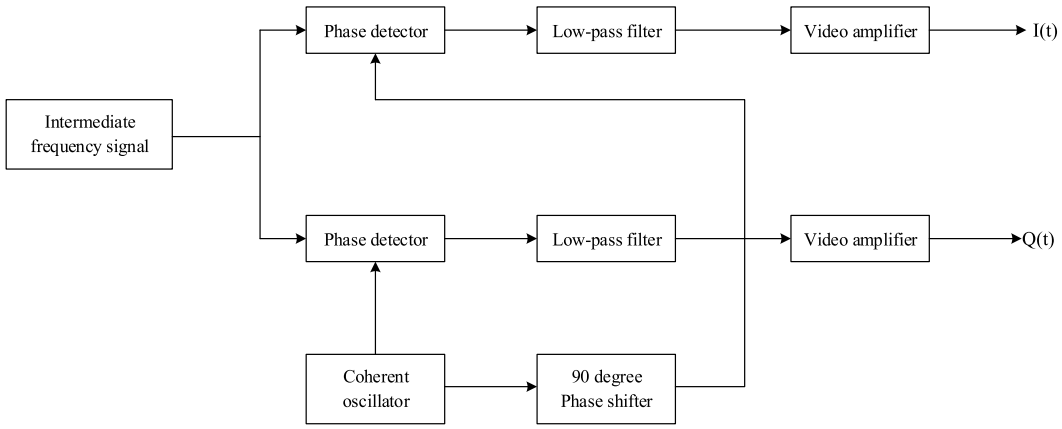

Fig. 3. Block diagram of orthogonal detector.

$$S_C(t) = S(t-\Delta\tau) \times S(t-\tau_1) \times S^*(t-\tau_1-\Delta\tau) \times a_{RCS} \times \exp\left[j(\varphi_{RCS}+\pi)\right] \tag{10}$$

Therefore, the cancellation signal for LFM signal can be obtained by substituting Eq. (3) into Eq. (10), the simplified formula form is

$$S_C(t) = S(t) a_{RCS} \exp\left[j(\varphi_{RCS}+\pi)\right] \exp(-j\pi\mu\tau_1\Delta\tau) \tag{11}$$

Similarly, substituting Eq. (5) into Eq. (10), we get the cancellation signal for Taylor [22]

$$\begin{aligned} S_C(t) = {} & S(t) \exp\left(-j\frac{B\pi}{T}\tau_1\Delta\tau\right) \\ & \times \exp\left(-jBT\sum_{n=1}^{N}\frac{A(n)}{n}\cos\left(\frac{n\pi}{T}(\Delta\tau-\tau_1)\right)\right) \\ & \times \exp\left(jBT\sum_{n=1}^{N}\frac{A(n)}{n}\cos\left(\frac{n\pi}{T}(\Delta\tau+\tau_1-2T)\right)\right) \\ & \times a_{RCS}\exp\left[j(\varphi_{RCS}+\pi)\right] \end{aligned} \tag{12}$$

Substituting Eq. (7) into Eq. (10), we attain the cancellation signal for combination of LFM and Tangent-FM

$$\begin{aligned} S_C(t) = {} & S(t) \exp\left[j\frac{B\pi}{T}(1-\alpha)\tau_1\Delta\tau\right] \times a_{RCS}\exp\left[j(\varphi_{RCS}+\pi)\right] \\ & \times \exp\left[j\frac{\pi\alpha BT}{2\gamma\tan\gamma} \times \left(\ln\left|\frac{1}{2}\left(\frac{1-\tan\frac{2\gamma t}{T}\cdot\tan\frac{2\gamma}{T}(t-\Delta\tau-\tau_1)}{\cos\frac{2\gamma t}{T}\times\cos\frac{2\gamma}{T}(t-\Delta\tau-\tau_1)}\times\cos\frac{2\gamma t}{T}(\tau_1-\Delta\tau)\right)\right|\right)\right] \end{aligned} \tag{13}$$

Finally, the cancellation signal for Stepped NLFM waveform can be achieved by substituting Eq. (9) into Eq. (10) as follows

$$\begin{aligned} S_C(t) = {} & S(t) \exp\left(j\frac{\pi B_L}{T}\tau_1\Delta\tau\right) \exp(j\pi B_C T\delta) \\ & \times a_{RCS}\exp\left[j(\varphi_{RCS}+\pi)\right] \end{aligned} \tag{14}$$

where $\delta = \cos\theta + \cos\phi - \cos\eta - \cos\upsilon$, θ, ϕ, η, υ can be got by the following

$$\begin{cases} t-\Delta\tau = T\sin\theta/2 \\ t-\tau_1 = T\sin\phi/2 \\ t = T\sin\eta/2 \\ t-\Delta\tau-\tau_1 = T\sin\upsilon/2 \end{cases} \tag{15}$$

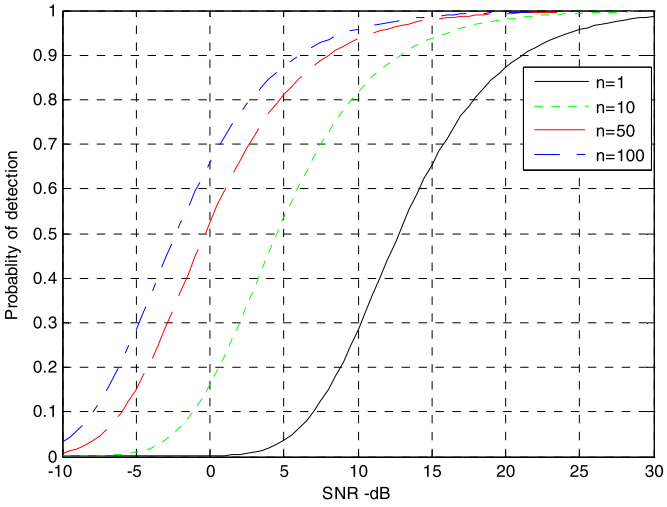

Fig. 4. Probability of detection versus SNR for Swerling I type target.

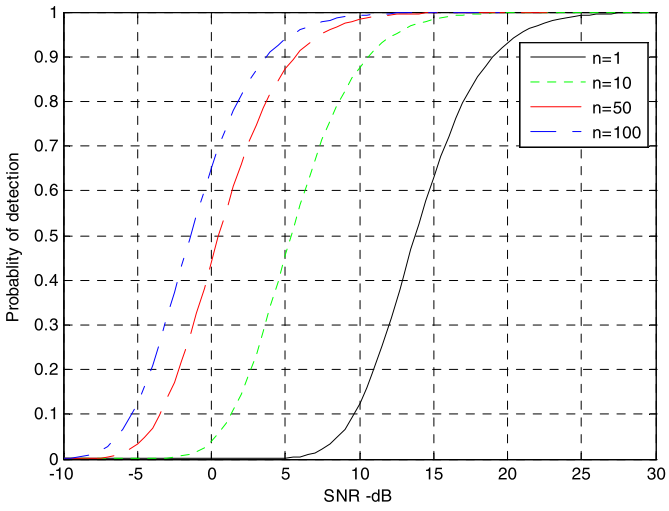

Fig. 5. Probability of detection versus SNR for Swerling III type target.

4. The detection probability for moving targets using Swerling models

This section discusses the radar detection probability for moving targets using Swerling I and III models. This work was first analysed by Marcum. Swerling extended Marcum's work to five distinct cases that account for variations in the target cross section. The main problem involving moving objects is its detection, which in turn lowers the signal-to-noise ratio (SNR). More details can be found in Ref. [16].

For Swerling I model Rayleigh probability distribution function is as follows

$$f(\sigma) = \frac{1}{\sigma}\exp\left(-\frac{\sigma}{\bar{\sigma}}\right), \quad \sigma \geq 0 \tag{16}$$

where $\bar{\sigma}$ is the average cross section value. For Swerling III type of target Rayleigh probability distribution function is expressed as

$$f(\sigma) = \frac{4\sigma}{\sigma^2}\exp\left(-\frac{2\sigma}{\bar{\sigma}}\right), \quad \sigma \geq 0 \tag{17}$$

As is known, the radar probability of detection (P_D) is a function of radar the SNR, threshold multiplier and false alarm probability P_{fa}. For the Swerling I model, we have

$$P_{fa} = 1 - \Gamma_1(V_T, n-1) \tag{18}$$

$$P_D = \begin{cases} \exp[-V_T/(1+SNR)], & n=1 \\ 1-\Gamma_1(V_T, n-1) \\ \quad +(1+\frac{1}{n\cdot SNR})^{n-1}\Gamma_1(\frac{V_T}{1+\frac{1}{n\cdot SNR}}, n-1), & n>1 \\ \quad \times \exp[-V_T/(1+n\cdot SNR)] \end{cases} \tag{19}$$

where V_T is the threshold voltage when noise alone is present in the radar, n is the number of pulses, $\Gamma_1(x,N) = \int_0^x \frac{\exp(-v)v^{N-1}}{(N-1)!}dv$ is called as incomplete gamma function. For instance, if $P_{fa} = 10^{-6}$, $n = 1, 10, 50, 100$, the relationship between detection probability P_D and SNR is shown in Fig. 4.

The radar detection probability for Swerling III model can be written as

$$P_D = \exp\left(\frac{-V_T}{1+n\cdot SNR/2}\right)\left(1+\frac{2}{n\cdot SNR}\right)^{n-2} \times K_0, \quad n = 1, 2 \tag{20}$$

where $K_0 = 1 + \frac{V_T}{1+n\cdot SNR/2} - \frac{2(n-2)}{n\cdot SNR}$. When $n > 2$, we have

$$P_D = \frac{V_T^{n-1}\exp(-V_T)}{(1+n\cdot SNR/2)(n-2)!} + 1 - \Gamma_1(V_T, n-1) + K_0 \times \Gamma_1\left(\frac{V_T}{1+2/n\cdot SNR}, n-1\right) \tag{21}$$

Fig. 5 shows the probability of detection as a function of SNR for different number of pulses where $P_{fa} = 10^{-9}$ in Swerling model III.

5. Amplitude, phase and frequency error analysis for the probability of detection

Due to the coherent wave interference principle, the radar echo is completely cancelled out when Eq. (22) are satisfied as follows [13]

$$\begin{cases} \Delta a = 0 \\ \Delta\varphi = (2k+1)\pi \\ \Delta f = 0 \end{cases} \tag{22}$$

where k is an integer, Δa is the amplitude error, $\Delta\varphi$ is the phase error, and Δf is the frequency error. However, there must be some errors in practical application. When $\Delta\tau$ and τ_1 satisfy some special conditions, the radar echo is cancelled by the interference wave, otherwise the radar echo is strengthened. Next, we will discuss the conditions which satisfy the cancellation.

Let $a_{RCS} = 1$ and $\varphi_{RCS} = 0$ as the simplified form, then the radar echo signal can be written as

$$S_e(t) = S(t) + S_C(t) \tag{23}$$

Substituting Eqs. (11)–(14) into Eq. (23), we can obtain the expressions of the LFM and NLFM echo signal which are shown in Table 2.

Considering the effect of amplitude, phase and frequency error on the probability of detection, the real signal normalized gain can be expressed as

$$\beta_{dB} = 20\lg\left[\left|1+(1+\Delta a)\cos(2\pi\Delta f t - \Delta\varphi + \pi)\right|\right] \tag{24}$$

Then we derive approximately the improved SNR from Eq. (24), it may be written as

$$SNR_L = 20\lg\left[\left|1+(1+\Delta a)\cos(2\pi\Delta f t - \Delta\varphi + \pi)\right| \cdot |SNR|\right] \tag{25}$$

Substituting Eq. (25) into Eq. (19), Eq. (20) and Eq. (21), we can get the cancelled radar detection probability which involves the ampli-

Table 2
The expression of the echo signal for LFM and NLFM.

Window function	Echo signal expression
LFM	$S_e(t) = S(t)\{1 + a_{RCS}\exp[j(\varphi_{RCS} + \pi)]\exp(-j\pi\mu\tau_1\Delta\tau)\}$
Taylor	$S_e(t) = S(t)\{1 + \exp(-j\frac{B\pi}{T}\tau_1\Delta\tau)\exp(-jBT\sum_{n=1}^{N}\frac{A(n)}{n}\cos(\frac{n\pi}{T}(\Delta\tau - \tau_1)))$ $\times \exp(jBT\sum_{n=1}^{N}\frac{A(n)}{n}\cos(\frac{n\pi}{T}(\Delta\tau + \tau_1 - 2T))) \times a_{RCS}\exp[j(\phi_{RCS} + \pi)]\}$
LFM & Tangent-FM	$S_e(t) = S(t)\{1 + \exp[j\frac{B\pi}{T}(1-\alpha)\tau_1\Delta\tau] \times a_{RCS}\exp[j(\phi_{RCS} + \pi)]$ $\times \exp\left[j\frac{\pi\alpha BT}{2\gamma\tan\gamma}\left(\ln\left|\frac{1}{2}\left(\frac{1-\tan\frac{2\gamma t}{T}\cdot\tan\frac{2\gamma}{T}(t-\Delta\tau-\tau_1)\times\cos\frac{2\gamma t}{T}(\tau_1-\Delta\tau)}{\cos\frac{2\gamma t}{T}\times\cos\frac{2\gamma}{T}(t-\Delta\tau-\tau_1)}\right)\right|\right)\right]\}$
Stepped	$S_e(t) = S(t)\{1 + \exp(j\frac{\pi B_I}{T}\tau_1\Delta\tau)\exp(j\pi B_C T\delta) \times a_{RCS}\exp[j(\phi_{RCS} + \pi)]\}$

Table 3
Probability of detection versus SNR for Swerling I, $n = 10$.

SNR (dB)	−10	−5	0	5	10	15	20	25	30
P_D (%)	0.019	0.985	16.105	53.539	81.648	93.740	97.971	99.353	99.795

Table 4
Probability of detection versus SNR for Swerling III, $n = 10$.

SNR (dB)	−10	−5	0	5	10	15	20	25	30
P_D (%)	0.000	0.016	3.920	45.516	87.644	98.341	99.817	99.981	99.998

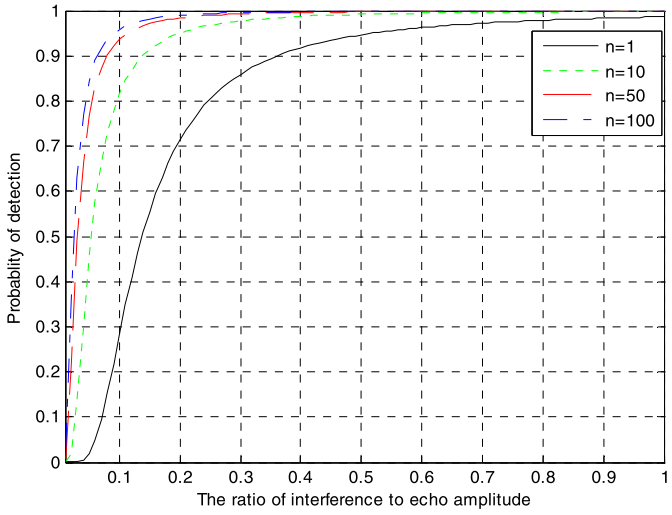

Fig. 6. Detection probability versus amplitude error for Swerling I.

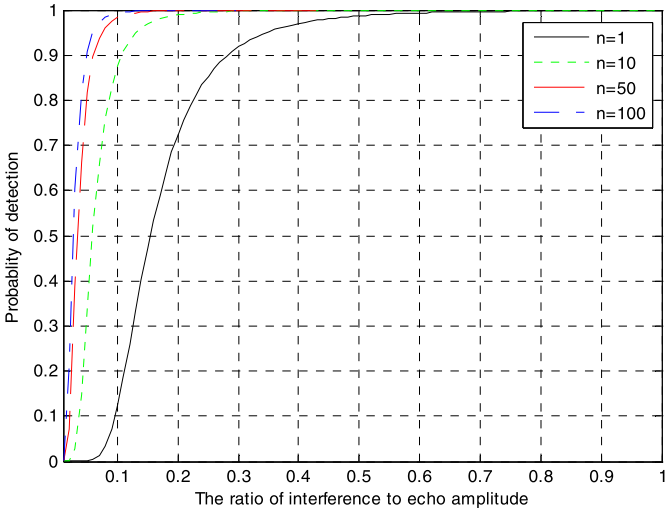

Fig. 7. Detection probability versus amplitude error for Swerling III.

tude error, phase error and frequency error. If we take $\Delta\varphi = 0$ and $\Delta f = 0$, then the improved SNR versus Δa becomes

$$SNR_{L-\Delta a} = 20\lg\left[|\Delta a| \cdot |SNR|\right] \tag{26}$$

Let $n = 10$, SNR=30 dB. From Table 3 and Table 4, the detection probability for Swerling I and Swerling III are $P_{D-I} \approx 99.795\%$ and $P_{D-III} \approx 99.998\%$ respectively.

Putting Eq. (26), Eq. (19) and Eq. (21) together, we acquire the cancelled radar detection probability versus amplitude error Δa which is shown in Fig. 6 and Fig. 7. The results are also shown in Table 5 and Table 6.

From Table 5, we can find $P_{D-I} \approx 99.795\%$ when $n = 10$, $\Delta a = 1$. That is to say, the radar detection probability will decrease when the amplitude error satisfies $0 < \Delta a \leq 1$, we call it partial cancellation under this circumstance. If $\Delta a > 1$, the radar detection

Table 5
Detection probability versus amplitude error for Swerling I, $n = 10$.

Δa	0.1	0.2	0.3	0.4	0.5	0.6	0.7	0.8	0.9	1
P_D (%)	81.648	95.014	97.748	98.946	99.183	99.432	99.582	99.680	99.747	99.795

Table 6
Detection probability versus amplitude error for Swerling III, $n = 10$.

Δa	0.1	0.2	0.3	0.4	0.5	0.6	0.7	0.8	0.9	1
P_D (%)	87.644	98.931	99.775	99.927	99.970	99.986	99.992	99.996	99.997	99.998

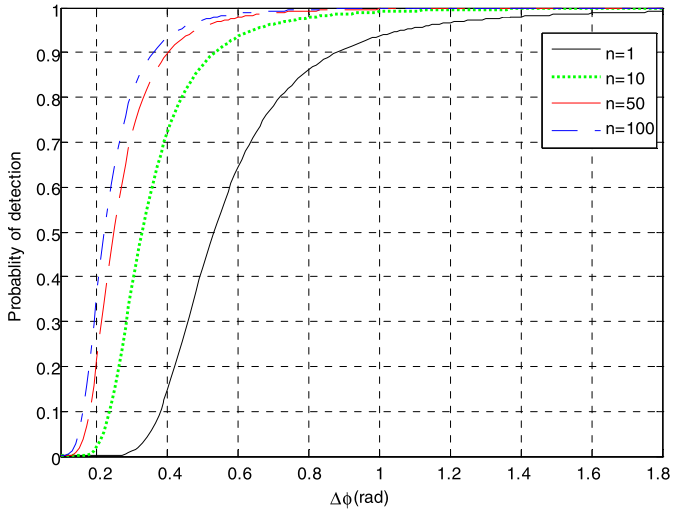

Fig. 8. Detection probability versus phase error for Swerling I.

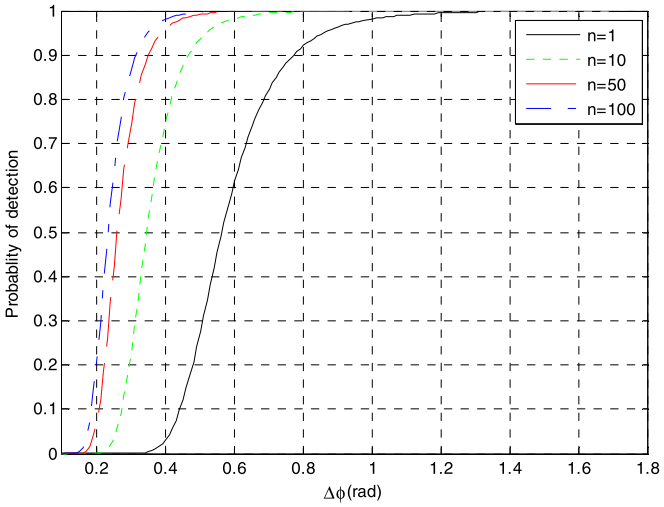

Fig. 9. Detection probability versus phase error for Swerling III.

Table 7
Detection probability versus phase error for Swerling I, $n = 10$.

$\Delta\varphi$	1.41	1.42	1.43	1.44	1.45	1.46	1.47	1.48	1.49
P_D (%)	99.763	99.768	99.772	99.777	99.782	99.786	99.790	99.795	99.799

Table 8
Detection probability versus phase error for Swerling III, $n = 10$.

$\Delta\varphi$	1.41	1.42	1.43	1.44	1.45	1.46	1.47	1.48	1.49
P_D (%)	99.998	99.998	99.998	99.998	99.998	99.998	99.998	99.998	99.999

Table 9
The relationship between $\Delta\varphi$ and τ_1, $\Delta\tau$ for LFM and NLFM.

Window function	$\Delta\varphi$ explicit expression
LFM	$\Delta\varphi = \pi\mu\tau_1\Delta\tau$
Taylor	$\Delta\varphi = \frac{B\pi}{T}\tau_1\Delta\tau + BT\sum_{n=1}^{N}\frac{A(n)}{n}\cos\left(\frac{n\pi}{T}(\Delta\tau-\tau_1)\right) - BT\sum_{n=1}^{N}\frac{A(n)}{n}\cos\left(\frac{n\pi}{T}(\Delta\tau+\tau_1-2T)\right)$
LFM & Tangent-FM	$\Delta\varphi = \frac{B\pi(1-\alpha)\tau_1\Delta\tau}{T} + \frac{\pi\alpha BT}{2\gamma\tan\gamma}\left(\ln\left\|\frac{1}{2}\left(\frac{1-\tan\frac{2\gamma t}{T}\cdot\tan\frac{2\gamma}{T}(t-\Delta\tau-\tau_1)\times\cos\frac{2\gamma t}{T}(\tau_1-\Delta\tau)}{\cos\frac{2\gamma t}{T}\times\cos\frac{2\gamma}{T}(t-\Delta\tau-\tau_1)}\right)\right\|\right)$
Stepped	$\Delta\varphi = \frac{\pi B_L}{T}\tau_1\Delta\tau + \pi B_C T\delta$

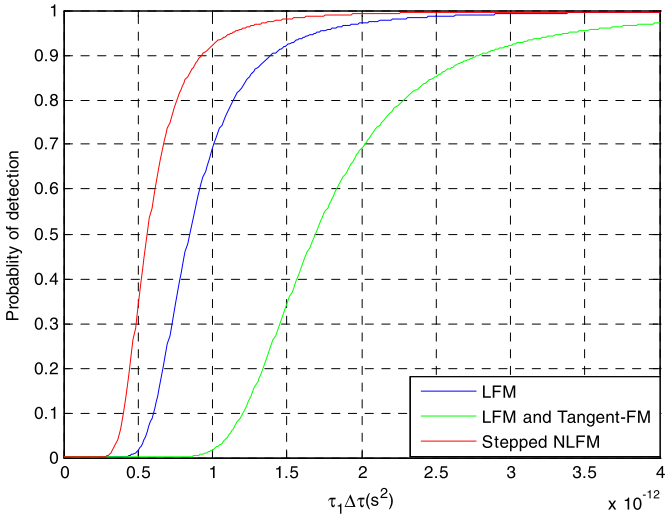

Fig. 10. Detection probability versus $\tau_1\Delta\tau$ phase error for Swerling I ($B = 10$ MHz, $T = 50$ μs, $\alpha = 0.5$, $n = 1$ and $B_L = 15$ MHz).

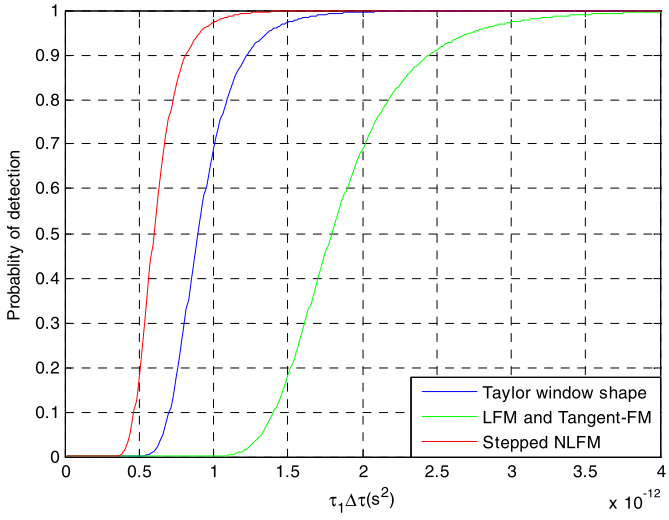

Fig. 11. Detection probability versus $\tau_1\Delta\tau$ phase error for Swerling III ($B = 10$ MHz, $T = 50$ μs, $\alpha = 0.5$, $n = 1$ and $B_L = 15$ MHz).

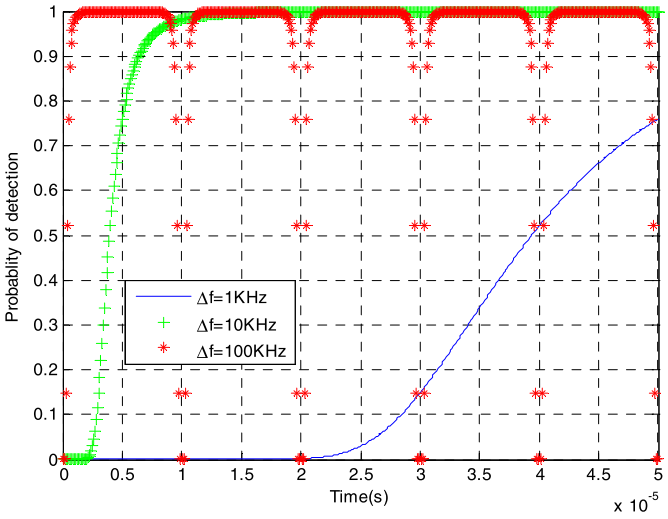

Fig. 12. Detection probability versus frequency error for Swerling I ($n = 50$).

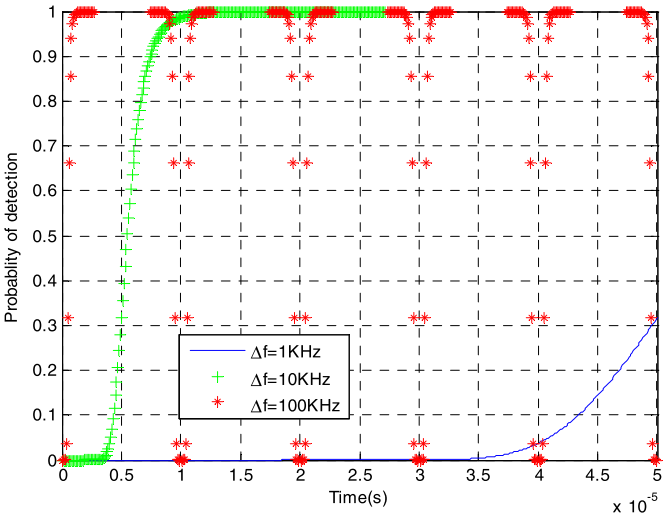

Fig. 13. Detection probability versus frequency error for Swerling III ($n = 10$).

probability will increase, then the radar echo will be strengthened. For the Swerling III, the same results may be obtained by taking a closer look at Table 6.

Likewise, if $\Delta a = 0$ and $\Delta f = 0$, the improved SNR versus phase error $\Delta\varphi$ will be

$$SNR_{L-\Delta\varphi} = 20\lg\left[\left|1-\cos(\Delta\varphi)\right|\cdot|SNR|\right] \tag{27}$$

Combining Eq. (27), Eq. (19) with Eq. (21), we obtain the cancelled radar detection probability versus phase error $\Delta\varphi$. Fig. 8 and Fig. 9 show how the cancelled radar detection probability varies with phase error. The results are also expressed in Table 7 and Table 8, partly.

From Table 7, we may know $P_{D-I} \approx 99.795\%$ when $n = 10$, $\Delta\varphi = 1.48$. Therefore, the radar detection probability will decrease when the phase error satisfies $0 < \Delta\varphi \leq 1.48$. Otherwise, the radar detection probability will increase when $\Delta\varphi > 1.48$, and the radar echo will be strengthened. For the Swerling III, the same results may be get through studying Table 8.

One the other hand, we can also calculate the relationship between $\Delta\varphi$ and τ_1, $\Delta\tau$ by using Table 2, the explicit expressions are shown in Table 9.

Suppose that there is only a phase difference of $\pi\mu\tau_1\Delta\tau$ in the LFM signal ($\frac{B\pi}{T}\tau_1\Delta\tau$ in the Taylor window shape NLFM signal, $\frac{B\pi(1-\alpha)\tau_1\Delta\tau}{T}$ in the LFM and Tangent-FM signal, or $\frac{\pi B_L}{T}\tau_1\Delta\tau$ in the Stepped NLFM signal). The phase errors of the LFM and NLFM signal are shown in Fig. 10 and Fig. 11.

In actual radar countermeasure, it is usually difficult to detect target when the radar detection probability fell below 50%, and therefore there is no need to cancel the echo signal completely. From Fig. 10 and Fig. 11, we can conclude that the radar detection probability will decrease to 50% by controlling the delay time

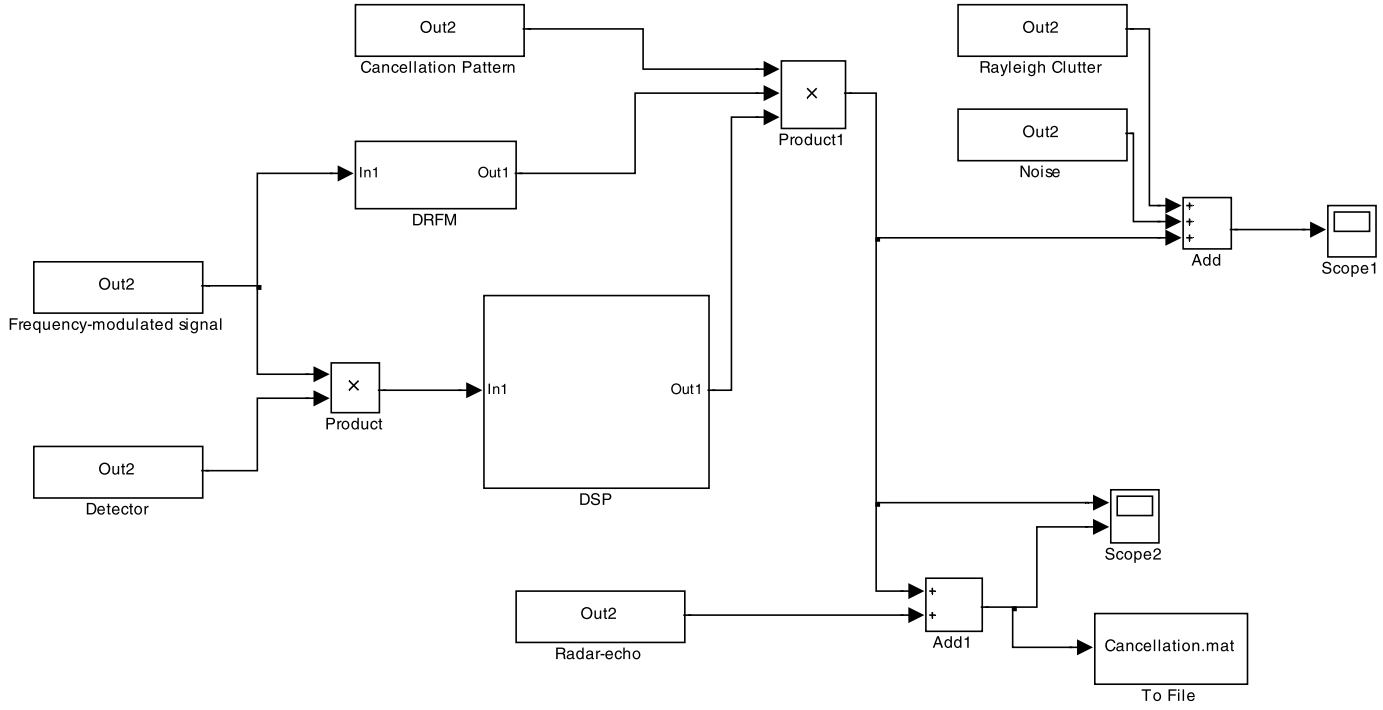

Fig. 14. The Simulink block diagram of simulation system.

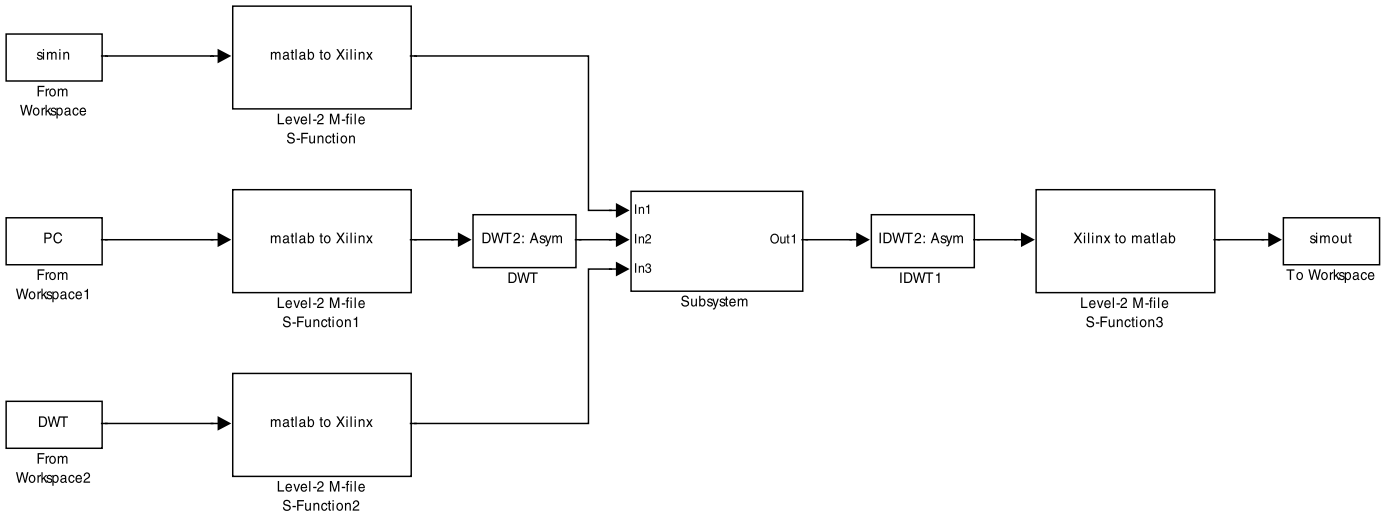

Fig. 15. The Simulink block diagram of signal processing.

$\tau_1 \Delta\tau$ for the LFM and NLFM signal, at this moment, we call it complete cancellation.

Finally, if we make $\Delta a = 0$ and $\Delta\varphi = 0$, the improved SNR versus frequency error Δf is expressed as

$$SNR_{L-\Delta f} = 20\lg\left[\left|1+\cos(2\pi\Delta f t+\pi)\right|\cdot|SNR|\right] \tag{28}$$

Substituting Eq. (28) into Eq. (19) and Eq. (21), we can get the cancelled radar detection probability versus frequency error Δf. Fig. 12 and Fig. 13 show how the radar detection probability varies versus frequency error.

From Fig. 12 and Fig. 13, we find that the radar detection probability shows periodic change. The bigger the frequency error is, the shorter is the periodic. In addition, the influence of frequency error on active cancellation is more sensitive than amplitude error and phase error.

6. Simulation of the cancelling system

According to the above theory, simulation experiments are carried out to verify the effect of active cancellation stealth for LFM and NFLM signal by using matlab/Simulink. The parameters are set as follows: LFM and NLFM signals carried impulse width is 50 μs, bandwidth is 10 MHz, amplitude error (the ratio interference to echo amplitude) is 0.4, frequency error 1 KHz, delay time is 2 μs. Fig. 14 shows the Simulink block diagram of the whole cancelling system. The Simulink block diagram of the signal processing among the system is shown in Fig. 15. The simulation results are shown in Fig. 16 and Fig. 17.

The simulation results show that using the above cancelling system can reduce the echo gain. In a certain error conditions, the system still has a very high cancellation effect. From Fig. 16(b), the signal amplitude is decreased about 15 dB. From Fig. 17(b), the signal amplitude is also decreased about 18 dB. Even in those error cases, the system can cancel the target echo effectively.

7. Conclusion

The results presented here may be summarized as follows: the radar detection probability is controlled effectively and efficiently through interaction between the cancellation signal and echo signal. The simulation results also indicate that using the cancelling system can reduce the echo gain. Even though there exist some errors, the system still have very high interference effect. Simultaneously, active cancellation stealth provides an effective supplement for the conventional stealth measures. Furthermore, using the radar detection probability, the extent of active cancellation can be classified as partial cancellation, complete cancellation

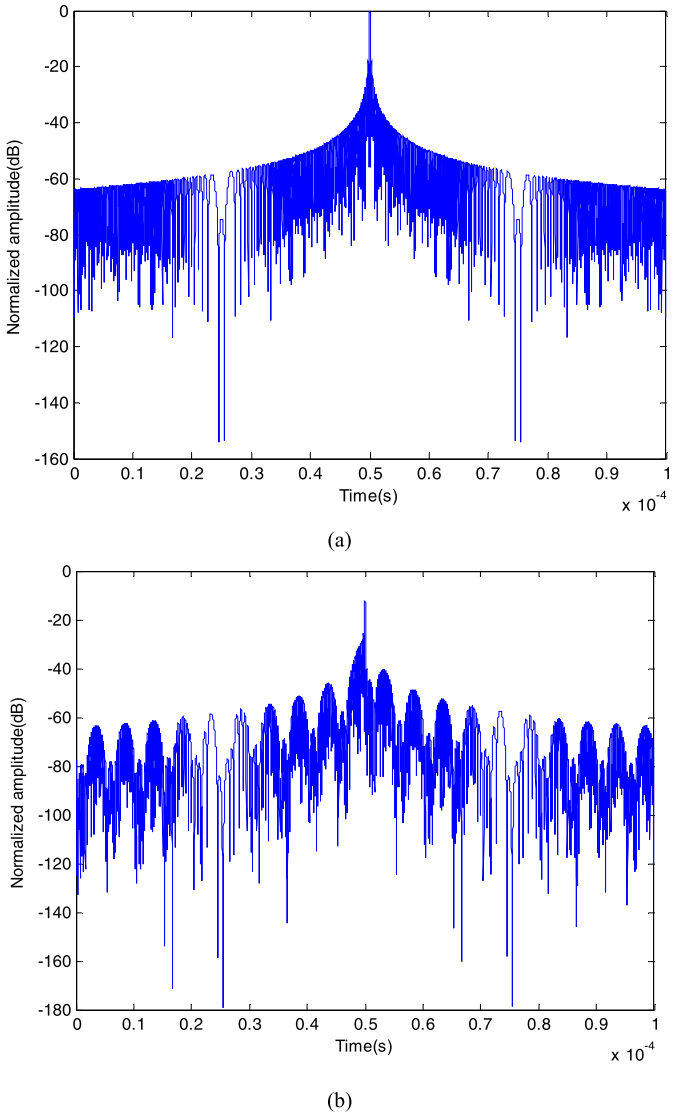

Fig. 16. (a) Before cancelling echo signal for LFM; (b) After cancelling echo signal for LFM.

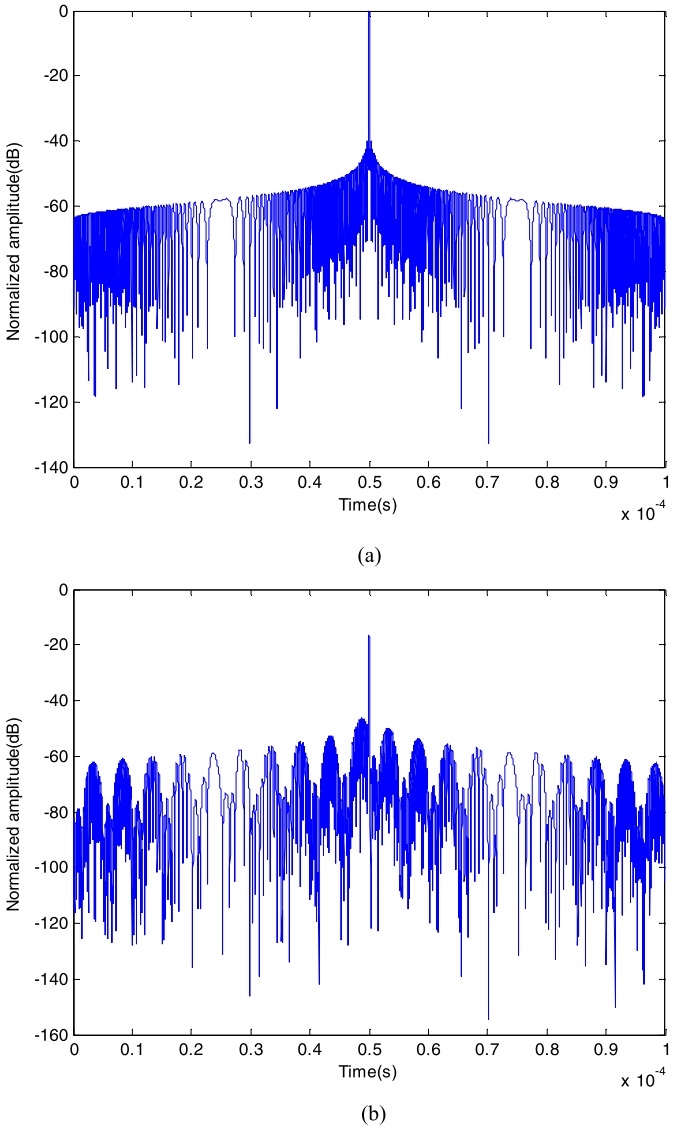

Fig. 17. (a) Before cancelling echo signal for Taylor window shape NFLM; (b) After cancelling echo signal for Taylor window shape NFLM.

and strengthening echo. Compared with Refs. [13] and [22], our method is more convenient to estimate stealth effect and to control some parameter errors.

Conflict of interest statement

None declared.

Acknowledgements

This work was supported by the National Natural Science Foundation of China under Grant No. 51307004.

References

[1] E.F. Knott, J.F. Shaeffer, M.T. Tuley, Radar Cross Section, SciTech Publishing, Inc., 2004.
[2] D.C. Jenn, Radar and Laser Cross Section Engineering, American Institute of Aeronautics and Astronautics Inc., 2005.
[3] C.W. Qu, Y.C. Xiang, Active cancellation stealth analysis based on RCS characteristic of target, Radar Sci. Technol. 8 (2) (2010) 109–112.
[4] C.W. Qu, Y.C. Xiang, H.P. Hou, W.J. Zhou, Cancellation interference analysis of coherent radar based on phase modulation, J. Univ. Electron. Sci. Technol. China 40 (6) (2011) 829–834.
[5] Y.C. Xiang, C.W. Qu, B.R. Li, H.P. Hou, Simulation research on cancellation stealth of warship based on its radar scattering properties, J. Syst. Simul. 25 (1) (2013) 104–110.
[6] Y.C. Xiang, C.W. Qu, D.F. Ping, W.Q. Zhao, Research on active cancellation stealth of warship, Ship Electron. Eng. 30 (2) (2010) 103–106.
[7] X. Guo, H.B. Sun, T.S. Yeo, Interference cancellation for high frequency surface wave radar, IEEE Trans. Geosci. Remote Sens. 46 (7) (2008) 1879–1892.
[8] K. Lizuka, A.P. Freundorfer, T. Iwasaki, A method of surface clutter cancellation for an underground CW radar, IEEE Trans. Electromagn. Compat. 31 (3) (1989) 330–332.
[9] B. Root, HF radar ship detection through clutter cancellation, in: IEEE National Radar Conference, Dallas, 1998, pp. 281–286.
[10] C. Paleologu, J. Benesty, et al., Widely linear general Kalman filter for stereophonic acoustic echo cancellation, Signal Process. 94 (2014) 570–575.
[11] S. Cecchi, L. Romoli, P. Peretti, F. Piazza, Low-complexity implementation of a real-time decorrelation algorithm for stereophonic acoustic echo cancellation, Signal Process. 92 (2012) 2668–2675.
[12] C. Stanciu, J. Benesty, et al., A widely linear model for stereophonic acoustic echo cancellation, Signal Process. 93 (2013) 511–516.
[13] Y.J. Wang, G.Q. Zhao, H.W. Wang, Echo cancelling algorithm for the LFM radar, J. Xidian Univ. 35 (6) (2008) 1031–1035.
[14] Y.C. Xiang, C.W. Qu, H.P. Hou, Y.K. Chen, Analysis of LFMICW cancellation based on group delay and ambiguity function, J. CAEIT 6 (2) (2011) 175–180.
[15] F.M. Dickey, C.S. Holswade, Laser Beam Shaping Theory and Techniques, Marcel Dekker Inc., New York, 2000.
[16] Z.J. Chen, Q. Luo, Q. Chen, Radar Systems Analysis and Design Using MATLAB, second edn., Publishing House of Electronics Industry, Beijing, 2008.
[17] Y. Li, N.R. Sollenberger, Adaptive antenna arrays for OFDM systems with co-channel interference, IEEE Trans. Commun. 47 (2) (1999) 217–229.
[18] P. Yichun, P. Shirui, et al., Optimization design of NLFM signal and its pulse compression simulation, in: IEEE Int. Conf. Radar, Arlington, 2005, pp. 383–386.
[19] T. Collins, P. Atkins, Nonlinear frequency modulation chirps for active sonar, IEE Proc. Radar Sonar Navig. 146 (6) (1999) 312–316.
[20] M. Luszczyk, Numerical evaluation of ambiguity function for stepped nonlinear FM radar waveform, in: Int. Conf. Microwaves Radar Wireless Commun., 2006, pp. 1164–1167.
[21] D.B. Adams, W.T. Snider, C.K. Madsen, A novel NFLM waveform generator using tunable integrated optical ring resonators: simulation and proof of concept experiment, Proc. SPIE 7684 (2010) 76841A-1–76841A-12.
[22] S. Xu, Y.M. Xu, Scheme for nonlinear frequency modulation signal cancelling system, Optik 124 (2013) 4896–4900.